

Bulk defect characterization in metalized solar cells using temperature-dependent Suns-V_{oc} measurements

Saman Jafari ^{a,*}, Malcolm Abbott ^a, Daqi Zhang ^b, Jian Wu ^b, Fangdan Jiang ^b, Ziv Hameiri ^a

^a The University of New South Wales, Sydney, NSW, 2052, Australia

^b Canadian Solar Inc, SND, Suzhou, 215129, China

ARTICLE INFO

Keywords:

Suns-v_{oc}
Ga-doped Cz silicon
Defect characterization
Light-induced degradation

ABSTRACT

Extracting the parameters, energy level and electron-to-hole capture cross-section ratio, of efficiency-limiting bulk defects in silicon solar cells is a critical step in identifying those defects and potentially eliminating their impact. Typically, this is achieved on specially prepared test structures. However, in some cases, this is not possible, especially in mass production lines when only completed solar cells are available. In this study, a method that is based on temperature-dependent Suns-V_{oc} measurements is introduced to extract the defect parameters in metalized solar cells. The method is validated by comparing the parameters of the boron-oxygen-related defect extracted from cells and those extracted from wafers using the commonly used temperature- and injection-dependent lifetime spectroscopy. It is shown that this method has the benefit of a more accurate lifetime at low injection levels compared with photoconductance-based lifetime measurement since it is not impacted by minority carrier traps. The proposed technique is then applied to determine the parameters of the defect causing light-induced degradation in gallium-doped silicon solar cells. We determined an energy level, with respect to the intrinsic level, of -0.26 ± 0.04 eV and a capture cross-section ratio of 34 ± 2 for this defect. Finally, a sensitivity analysis is performed by considering the system's limited measurement temperature range. The findings demonstrate the potential of the temperature-dependent Suns-V_{oc} method as a fast and easy-to-apply method for defect characterization in metalized cells.

1. Introduction

Temperature- and injection-dependent lifetime spectroscopy (TIDLS) has been widely used to extract the energy level (E_i) and the electron-to-hole capture cross-section ratio (k) of defects in silicon wafers [1–5]. In this method, the effective lifetime is measured across a wide range of excess carrier concentrations (injections) at different temperatures [6]. The defect parameters are then extracted by fitting the obtained lifetime curves at each temperature using the Shockley-Read-Hall (SRH) equation [6–8]. Despite some limitations [6] TIDLS allows the determination of parameters for the lifetime-limiting defects, even in the cases of very low defect concentration [1]. Commonly, the quasi-steady state photoconductance (QSSPC) and transient photoconductance measurement methods are used for lifetime measurements [9,10]. However, samples with a significant amount of metal on the surface (i.e. solar cells) cannot be measured using this method. One approach to overcome this barrier is to use wafers, that closely match those used for the cells (*sister* wafers), to study the defect. However, sister wafers are not always available in

production lines and the preparation of these wafers often requires significant effort. Another possible method for lifetime measurement on metalized cells is front detection QSS-photoluminescence (PL) measurement [11,12]. However, this method needs a sophisticated calibration for each sample, thus, it is not suitable for production lines. Hence, there is a need to develop a fast method, that can be easily used in a production environment, to extract defect parameters directly from solar cells.

The illumination-open circuit voltage (V_{oc}) measurement, also known as Suns-V_{oc}, has been long used as a method to obtain solar cell's pseudo-current-voltage (I-V) parameters without the impact of the series resistance [13]. The method is based on the measurement of V_{oc} at different illumination intensities that are easily converted to current. Importantly, lifetime curves can also be extracted from Suns-V_{oc} measurements and unlike PC-based lifetime measurements, the obtained lifetime is not overestimated by artifacts that impact the low injection levels (such as minority carrier traps [14] and depletion region modulation [15]). While temperature-dependent Suns-V_{oc} measurements of

* Corresponding author.

E-mail address: s.jafari@student.unsw.edu.au (S. Jafari).

silicon-based solar cells have been used in a few studies [16–18] they have not been utilized for TIDLS-like defect characterization.

In this study, a method based on temperature-dependent Suns-V_{oc} [Suns-V_{oc}(T)] is used to extract the defect parameters in metalized cells. The method is first validated by comparing the parameters of the well-known boron-oxygen (BO)-related defect [1,19] extracted from solar cells and lifetime structures fabricated from boron-doped Czochralski (Cz) wafers. We then investigate light-induced degradation (LID) in gallium (Ga)-doped cells and wafers. Ga has recently replaced boron (B) as the dopant in p-type wafers which are used for photovoltaic applications [20]. Although some studies indicated that there is no LID in Ga-doped cells [21] recent investigations have reported that some Ga-doped wafers degrade under illumination [22,23]. Nevertheless, the nature of the defect responsible for this degradation has not yet been determined. Using the proposed Suns-V_{oc}(T) method, we extract the parameters of the defect causing the degradation in commercial Ga-doped passivated emitter and rear solar cells (PERC). Finally, we perform a sensitivity analysis of the method to investigate the effect of a limited temperature range on the certainty of extracted parameters.

2. Materials and methods

Sets of B- and Ga-doped wafers (B: $1.8 \pm 0.05 \Omega \cdot \text{cm}$; $167 \pm 2 \mu\text{m}$, Ga: $1.9 \pm 0.05 \Omega \cdot \text{cm}$; $189 \pm 2 \mu\text{m}$) and cells (B: $0.8 \pm 0.02 \Omega \cdot \text{cm}$; $200 \pm 5 \mu\text{m}$, Ga: $0.7 \pm 0.02 \Omega \cdot \text{cm}$; $205 \pm 5 \mu\text{m}$) were used in this study. The wafers were gettered using a phosphorus diffusion process at 840°C for 45 min. The diffused layer was subsequently removed using a hydrofluoric acid-nitric acid solution with a ratio of 1:10. The wafers were then passivated with 75 nm silicon nitride (refractive index of 2.08 at 632 nm) using a plasma-enhanced chemical vapor deposition (PECVD) system [24]. They were later fired at sample peak temperatures of 700°C . The cells were commercially produced bifacial PERC cells (both B- and Ga-doped), passivated with an industrial PECVD-based SiN_x passivation (front: SiO_x-SiN_x; rear: AlO_x-SiN_x).

The degradation was performed by light-soaking either at 130°C using halogen lamps with 0.4 Suns equivalent photon flux illumination intensity (wafers) or at 130°C using a 960 nm laser with 40 Suns intensity (cells). The extent of degradation at each stage was monitored using PL imaging. Prior to the degradation, the B-doped cells were dark annealed at 220°C for 20 min to destabilize the BO-related defect [19].

TIDLS measurements of the wafers were done using our custom-made temperature-dependent lifetime system [25]. The lifetime was monitored before and after the TIDLS (at 30°C) to verify that no change was induced by the measurements. In this study, the reported lifetime is the average of ten consecutive measurements. A modified Suns-V_{oc} system (Fig. 1) was used to measure the cells. The system allows measurements in the temperature range of 25°C to 200°C . An X5DR flash head from Quantum Instruments was used as the excitation source. Similar to the wafers, Suns-V_{oc} measurements at 30°C were performed before and after the temperature-dependent measurements to verify that no changes are induced during the measurements. As pre-tests indicated that averaging has only a negligible impact on the quality of the measurement, no averaging was used for the Suns-V_{oc} measurements.

As discussed, the effective lifetime (τ_{eff}) can be extracted from Suns-V_{oc} measurements. The excess carrier density (Δn) was extracted using [26]:

$$\Delta n(N_D + \Delta n) = n_i^2 \exp\left(\frac{V_{\text{oc}}q}{k_B T}\right) \quad (1)$$

where N_D is the doping concentration, n_i is the intrinsic carrier concentration, q is the elementary charge, k_B is the Boltzmann constant, and T is the temperature in Kelvin. In this study, the model introduced by Couderc et al. is used to determine n_i [27]. Using the system's reference cell to determine the generation rate (G), τ_{eff} can then be calculated:

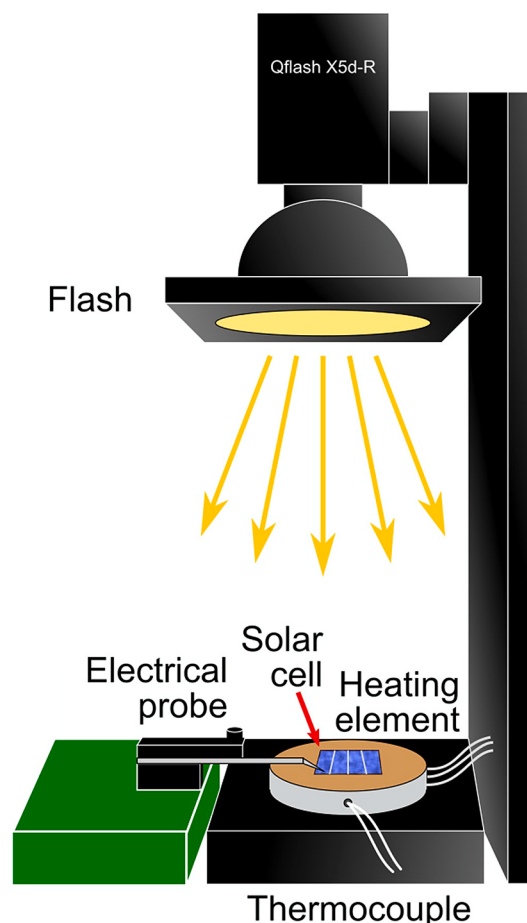


Fig. 1. Schematic of the modified Suns-V_{oc} system for temperature-dependent Suns-V_{oc} measurements.

$$\tau_{\text{eff}} = \frac{\Delta n}{G - \frac{d\Delta n}{dt}} = \frac{\Delta n}{J_{sc}S - \frac{d\Delta n}{dt}} \quad (2)$$

where J_{sc} is the short circuit current density of the cell at 1 Sun illumination, S is the illumination intensity which is determined using the reference cell, w is the cell thickness, and t is the time. To account for the change in G with temperature, J_{sc} should be known at each temperature. In this study, J_{sc} was measured using a SINUS-220 I-V tester from WaveLabs at eight temperatures in the 25°C to 60°C range. The temperature coefficient of J_{sc} was extracted from the linear fit to determine its value at any given temperature.

The SRH lifetime of the dominant defect (LID-related defect) was determined from the measured lifetime before and after the degradation using:

$$\frac{1}{\tau_{\text{eff(not-degraded)}}} = \frac{1}{\tau_{\text{surface}}} + \frac{1}{\tau_{\text{intrinsic}}} + \frac{1}{\tau_{\text{other}}} \quad (3)$$

$$\frac{1}{\tau_{\text{eff(degraded)}}} = \frac{1}{\tau_{\text{surface}}} + \frac{1}{\tau_{\text{intrinsic}}} + \frac{1}{\tau_{\text{LID}}} + \frac{1}{\tau_{\text{other}}} \quad (4)$$

where $\tau_{\text{eff(not-degraded)}}$ ($\tau_{\text{eff(degraded)}}$) is the effective lifetime in the not-degraded (degraded) state, τ_{surface} is the surface-related lifetime, $\tau_{\text{intrinsic}}$ is the intrinsic lifetime, τ_{LID} is the LID-related SRH lifetime, and τ_{other} is the lifetime related to all other factors. It should be noted that the effect of all the other defects (except for the LID-related defect) is considered in the τ_{other} term. By determining the harmonic difference between Eqs. (3) and (4), τ_{LID} can be isolated. It should be noted that this

procedure is not always necessary when wafers are investigated, however, it is often crucial for cells as τ_{other} (and τ_{surface}) in cells can be similar in magnitude to the investigated defect [28–30]. Thus, it is highly important to remove these effects by subtracting their contribution to the effective lifetime (here it is assumed that they are not modified by the degradation process).

3. Results and discussion

3.1. Investigation of the BO-related defect in cell

Fig. 2 presents the lifetime (at 30 °C) of a wafer (a) and a cell (b) before and after degradation, as well as the extracted LID-related SRH lifetime. As expected, the lifetime dropped after the light-soaking process, mainly at low injection levels [6]. At $\Delta n = 10^{15} \text{ cm}^{-3}$, the lifetime reduced by 65% (wafer) and 19% (cell). The difference in the degradation extent can be explained by the different initial lifetimes. The lower initial lifetime of the cells is probably due to recombination in the heavily diffused regions and poorer surface passivation (as state-of-the-art laboratory-type surface passivation has been used for the wafers compared to inline passivation for processed cells). The different degradation extent can also be attributed to the different doping densities and different firing conditions as it is known that the firing process can suppress the generation of BO-related defects [31]. **Fig. 2** highlights an important benefit of the proposed method. Note the high quality of the lifetime measurements down to $\Delta n = 10^{13} \text{ cm}^{-3}$ obtained via the Suns-Voc measurement [**Fig. 2(b)**]. In comparison, the PC-based measurements [**Fig. 2(a)**] seem to be impacted by artifacts below $\Delta n = 2 \times 10^{14} \text{ cm}^{-3}$, limiting the range of data available for subsequent extraction of the defect parameters (marked with a square).

Fig. 3(a) shows the defect parameter solution surface (DPSS) curves [6] corresponding to the BO-related SRH lifetime in the range of –25 °C to 100 °C for a B-doped wafer. **Fig. 3(c)** presents the standard deviation of the fitted k across all the temperatures at each energy level, where the energy level is reported relative to the intrinsic energy (E_i). The black dots at each bandgap half in **Fig. 3(a)** are the $[E_t, k]$ combinations that provide the lowest normalized standard deviation of k . **Fig. 3(b)** and (d) are similar graphs for the B-doped cell measured in the range of 30 °C to 90 °C by the Suns-Voc(T) system. Since the lifetime of the cell starts to recover at temperatures higher than 90 °C, the upper bound of the measurement is limited to this temperature. In both cases of the wafer and cell, the intersection point between the DPSS curves is not very sharp. We assume it is due to the temperature dependence of k resulting from the temperature dependence of the capture cross-sections and uncertainty in measurements. Therefore, the lower standard deviation associated with $[E_t, k]$ of the cell compared to the wafer can be explained by the smaller temperature range in the Suns-Voc(T) measurement.

The extracted defect parameters, $[E_t, k]$, for the wafer and cell are

summarized in **Table 1**. The reported uncertainty for the k values is the standard deviation of the DPSS curves at each solution. For energy level, it is reported as the uncertainty corresponding to the uncertainty in k . As mentioned before, these uncertainties are due to the temperature dependence of k and possible measurement noise. Good agreement is obtained between the extracted E_t . Furthermore, the extracted E_t in the upper half is similar to the E_t reported in Ref. [1] and slightly higher than the E_t determined by Ref. [32]. Regarding the extracted k values for the wafer and cell, a small difference in both bandgap halves can be observed. The difference between the extracted k values can be explained by the lower degradation extent in the case of the cell. The harmonic difference between the lifetime of the two states (not-degraded and degraded) is quite small and therefore is prone to measurement uncertainty. Another possible reason for this difference is the smaller temperature range in the Suns-Voc(T) system. The uncertainty associated with this limited temperature range will be investigated in Section 3.3. It will be shown that the smaller temperature range is not the source of the observed difference in the extracted k values. Compared with the literature, the value extracted from the wafer is slightly lower than the k reported by Ref. [1] and in the range reported in Ref. [32]. For the cell, the extracted k value is higher than the values reported in both studies (18–25% higher) [1,32]. Overall, the extracted value of k agrees with the literature within the expected uncertainty of the various methods. These results demonstrate the potential of the proposed method to extract the defect parameters *directly* from solar cells. Hence, it can be used in solar cell production lines without the need for sister wafers or special sample preparation.

3.2. Investigation of light-induced degradation in Ga-doped cell

As discussed, Ga has become the dominant doping element for p-type silicon wafers for photovoltaic applications [20]. To improve the stability of solar cells fabricated on Ga-doped substrates, it is important to investigate the defect causing LID in this material. **Fig. 4** shows the lifetime (at 30 °C) of a Ga-doped wafer (a) and cell (b) before and after LID, as well as the LID-related lifetime. At $\Delta n = 10^{15} \text{ cm}^{-3}$, the lifetime reduces by 60% (wafer) and 8% (cell; 17% at 10^{14} cm^{-3}).

Fig. 5(a) and (c) present the DPSS curves and the corresponding standard deviation curve as a function of energy level for a representative Ga-doped Cz wafer while **Fig. 5(b)** and (d) show similar graphs for the cell. **Table 2** summarizes the extracted $[E_t, k]$. The extracted energy levels from the wafer and the cell match well in the bottom bandgap half. However, in the upper bandgap half, the values have a larger difference. This is partially related to the difference in the measurement temperatures [6]. Since in both structures, the extracted energy level at the bottom bandgap half has a lower standard deviation, it can be suggested that this is the more likely solution. The extracted k values in both bandgap halves are slightly different (~30%) which might be due to the

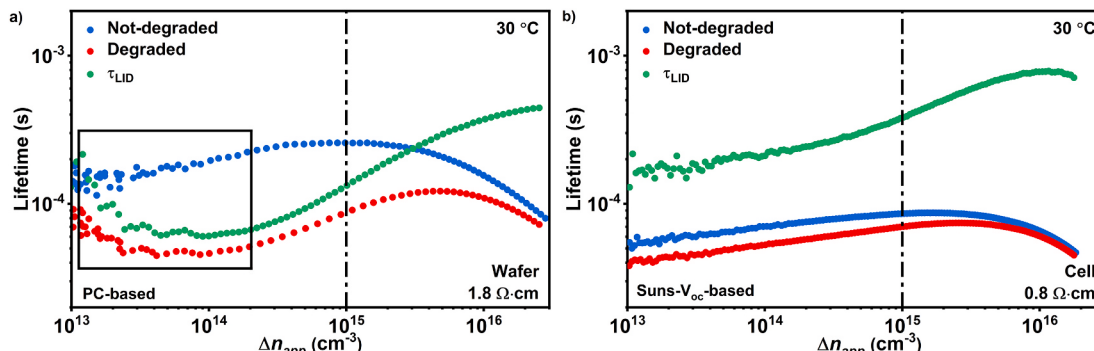


Fig. 2. Lifetime measurements at 30 °C of a B-doped wafer measured with the PC-based method (a) and cell measured with the Suns-Voc-based method (b) before (blue) and after (red) degradation, and the LID-related (green) lifetime curves. (For interpretation of the references to colour in this figure legend, the reader is referred to the Web version of this article.)

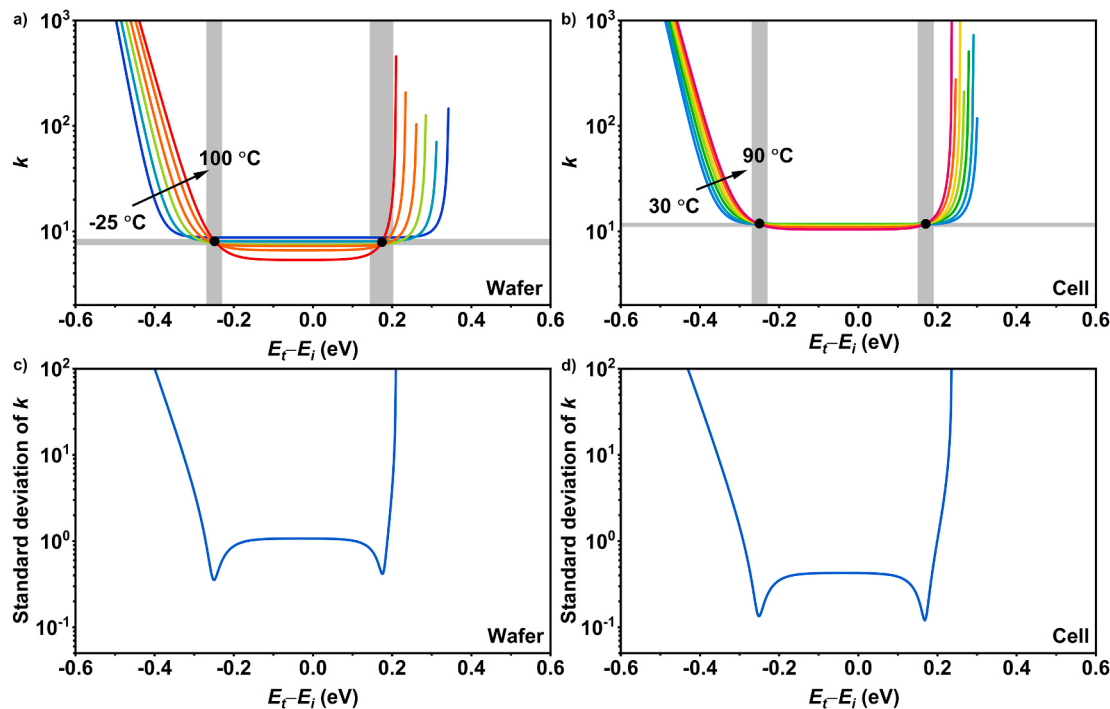


Fig. 3. Top row: DPSS curves of k for BO-related defect in a wafer (a) and cell (b). Bottom row: Standard deviation of the DPSS curves at each energy level for the wafer (c) and cell (d). The black dots are the calculated defect parameters. The shaded areas indicate the uncertainty range associated with the fitting process. (For interpretation of the references to colour in this figure legend, the reader is referred to the Web version of this article.)

Table 1

Energy level and capture cross-section ratio for BO-related defect in a wafer, a cell, and previously reported values.

Bandgap half	Parameter	Wafer	Cell	Ref. [1]	Ref. [32]
Bottom	$E_t - E_i$ (eV)	-0.25 ± 0.02	-0.25 ± 0.02	-	-0.22 to 0
	k	8.1 ± 0.4	11.9 ± 0.2	-	5–10
Upper	$E_t - E_i$ (eV)	0.17 ± 0.03	0.17 ± 0.02	0.15 ± 0.04	0 to 0.12
	k	7.9 ± 0.5	11.8 ± 0.2	9.5	5–10

factors mentioned previously (lower degradation extent in the case of the cell and different measurement temperature range). To separate the impact of different sources of error on the extracted parameters, the DPSS curves in the 25 °C to 100 °C (wafer) and 30 °C to 105 °C (cell) temperature ranges are compared. The results suggest that by changing

the temperature ranges, the difference in the extracted E_t is slightly reduced, while the difference in k is slightly increased. These results suggest that the main source of error for the investigated defect is the temperature-dependence of k when extracting E_t and the extent of the degradation when extracting k .

The $[E_t, k]$ combination of defects with similar E_t or k values are also shown in Fig. 5(a) and (b). In the bottom bandgap half, the best matches are light- and elevated temperature-induced degradation (LeTID)-related defect [4] $\text{Ti}_i^{+/++}$ [34] and $\text{Mo}_i^{0/+}$ [36]. In the upper bandgap half, the best match for the wafer is the LeTID-related defect while no good match can be found for the cell. It is noted that a k of around 34 was recently reported for the LeTID-related defect in Ga-doped Cz silicon [37] which agrees with our findings (however, as they did not use TIDLS, the energy level has not been reported). Despite the good agreement between the extracted parameter in the bottom half with the parameters of the LeTID-related defect, it has been indicated that the degradation of Ga-doped cells may not have the typical behavior of LeTID after dark annealing and stabilization processes [23]. Hence,

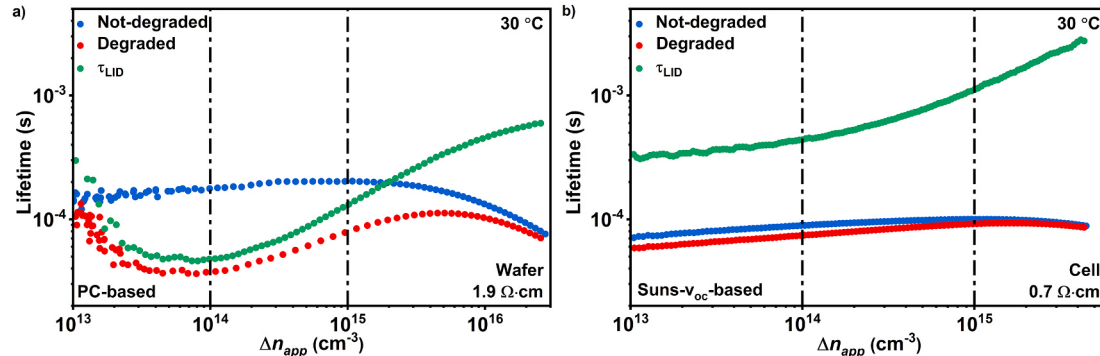


Fig. 4. Lifetime measurements at 30 °C of a Ga-doped wafer measured with the PC-based method (a) and cell measured with the Suns- V_{oc} -based method (b) before (blue) and after (red) degradation, and the LID-related (green) lifetime curves. (For interpretation of the references to colour in this figure legend, the reader is referred to the Web version of this article.)

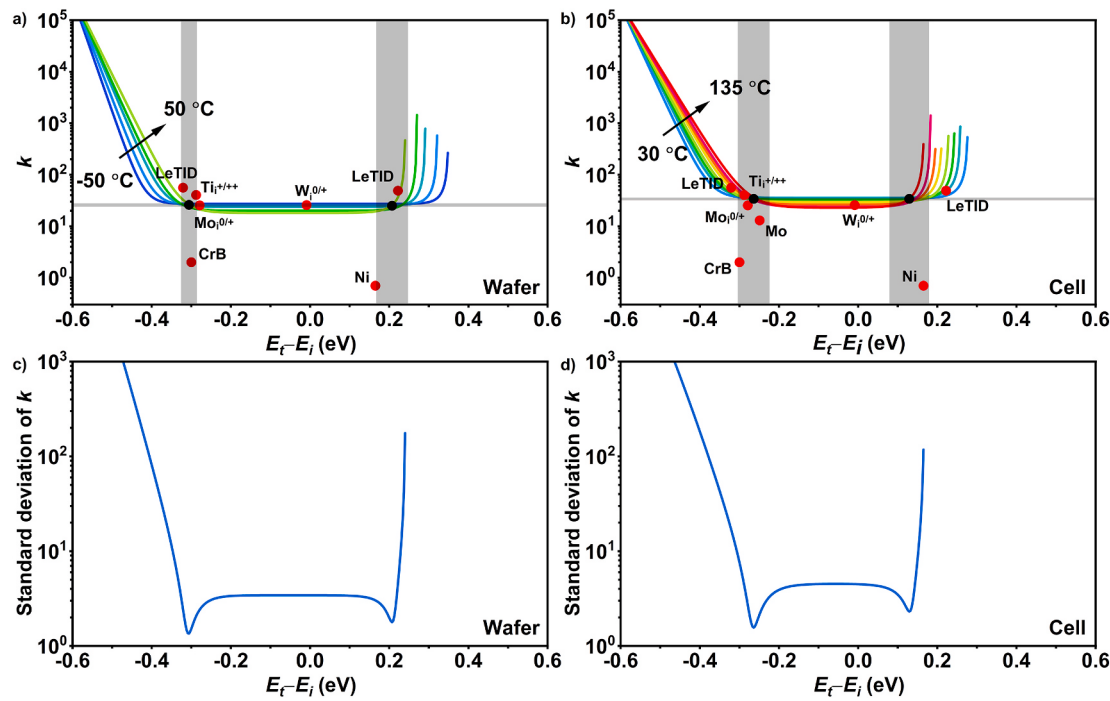


Fig. 5. Top row: DPSS curves of the k for LID-related defect in a Ga-doped wafer (a) and cell (b). Bottom row: Standard deviation of the DPSS curves at each energy level for the wafer (c) and cell (d). The black dots are the calculated defect parameters. The shaded areas indicate the uncertainty range associated with the fitting process. Candidate defects with parameters from the literature are plotted as red dots [4,33–36]. (For interpretation of the references to colour in this figure legend, the reader is referred to the Web version of this article.)

Table 2

Energy levels and capture cross-section ratios for LID-related defect as extracted from the Ga-doped wafer, cell, and values reported for LeTID-related defect parameters.

Bandgap half	Parameter	Wafer	Cell	LeTID [4]
Bottom	$E_t - E_i$ (eV)	-0.31 ± 0.02	-0.26 ± 0.04	-0.31 ± 0.05
	k	26 ± 2	34 ± 2	46 ± 16
Upper	$E_t - E_i$ (eV)	0.21 ± 0.04	0.13 ± 0.05	0.21 ± 0.05
	k	25 ± 2	33 ± 3	45 ± 15

further investigation is required to determine if this defect is similar to the LeTID-related defect.

3.3. Sensitivity analysis of the Suns-V_{oc}(T) measurement for defect characterization

The main limitation of the Suns-V_{oc}(T)-based TIDLS technique used in this study, compared to the common lifetime-based TIDLS, is the limited temperature range of the tool; particularly the inability to perform measurements below 30 °C. Note that this is not a fundamental limitation of the technique and can be removed by integrating a cooling stage into the system. The possibility of introducing a systematic error in the extracted parameters due to this limitation is discussed in this section.

The systematic error is investigated by modeling the injection-dependent lifetime curves with added artificial noise. SRH lifetime curves of a wafer with doping of $2.25 \times 10^{16} \text{ cm}^{-3}$ (similar to the Ga-doped cells) were generated for 11,500 $[E_t, k]$ combinations within the $E_t - E_i$ range of -0.57 eV to 0.57 eV and k of 0.01 to 100. Random Gaussian noise was added to the generated data with noise that is anticorrelated with the injection level (see Appendix A). Using the simulated lifetime graphs, DPSS curves at different temperatures were created and the defect parameters were extracted in each bandgap half. The error associated with the extracted parameters was then determined

from the comparison to the input values. This procedure was repeated 50 times for each $[E_t, k]$ combination and the averaged error is reported in the following figures. For E_t , the error is reported in eV (absolute error) while the percentage is used to report the error for k (relative error). The simulation has been performed in three temperature ranges: (a) 30 °C to 90 °C (15 °C intervals) to consider the cases where bulk lifetime is overly sensitive to high-temperature measurements [similar to the Suns-V_{oc}(T) measurements of the B-doped cell]; (b) 30 °C to 135 °C (15 °C intervals) as the typical temperature range of our Suns-V_{oc}(T) system; and (c) -30 °C to 135 °C (15 °C intervals) to represent the temperature range of a lifetime-based TIDLS measurement. It should be noted that the reported error in this section is different from the reported uncertainty (Figs. 3 and 5). Since the real value is known, the calculated error is the difference between the real value and the extracted value. The uncertainty, on the other hand, is the confidence interval associated with the experimental data. It is due to both noise in measurements and temperature-dependence of k , while for the error, only the noise is considered. Note that with no noise, the correct solution is determined across the entire simulated $[E_t, k]$ space (i.e. no error).

Fig. 6 presents the error map of E_t [(a), (b), and (c)] and k [(d), (e), and (f)] for the simulated lifetime curves. The $[E_t, k]$ for the BO-related defect extracted from the B-doped cell (in the upper bandgap half) is shown as a white circle while the $[E_t, k]$ of the LID-related defect extracted from the Ga-doped cell (in the bottom bandgap half) is shown as a red circle.

The general trend of the error maps for both E_t and k are similar for all three cases. In general, near the mid-gap, the error of the extracted E_t is higher than in other areas. The high error associated with defect parameter extraction near mid-gap has been previously reported [38]. For k , the region near the mid-gap with k between ~0.1 and ~50 has a low error while outside this region, especially near the band edges, the error is relatively high.

Comparing Fig. 6(a) and (b), it seems that increasing the upper band of the temperature range from 90 °C to 135 °C reduces the error across the entire simulated range, especially for defects near the mid-gap.

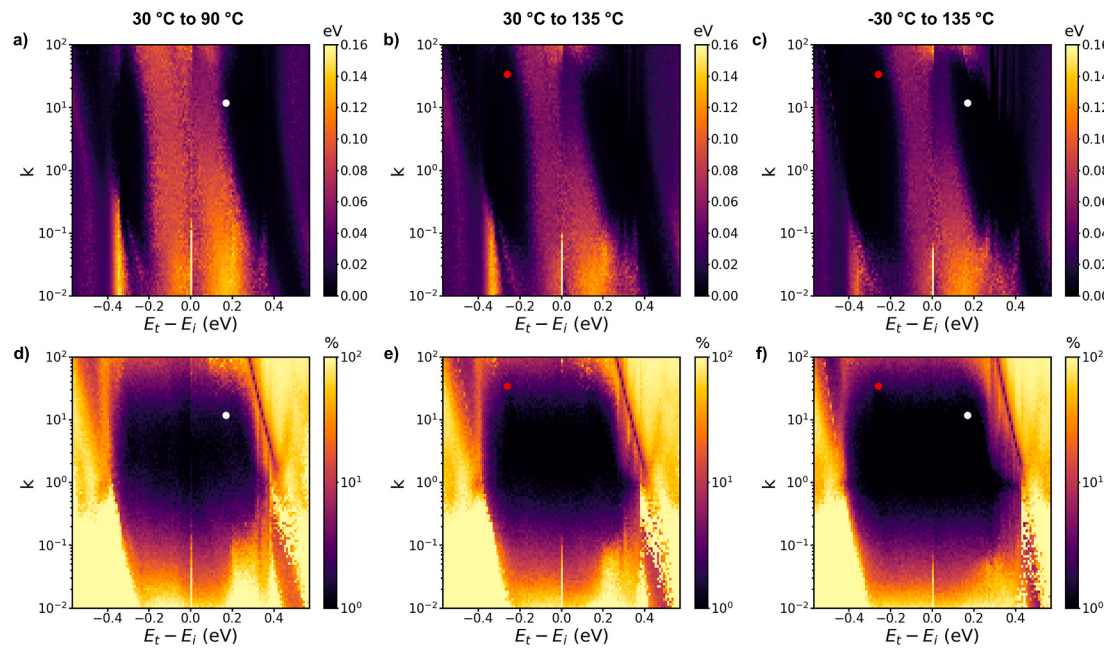


Fig. 6. Map of the absolute error in the extracted E_t (a, b, c) and relative error in the extracted k (d, e, f) as a function of $E_t - E_i$ and k for the simulated lifetime measurements in the temperature ranges of 30 °C to 90 °C (a, d), 30 °C to 135 °C (b, e), and -30 °C to 135 °C (c, f).

Extending the lower bound of the measurement temperature further increases the accuracy of the extracted energy level, mainly near the band edges [compare Fig. 6(b) and (c)].

The error maps of k show a similar trend; a wider temperature range lowers the error across the entire range. The high-accuracy region of k (dark areas in the figures) is further expanded when the measurements are extended to lower temperatures. It is interesting to notice that k can be extracted with a high level of accuracy around mid-gap, despite the large error associated with E_t . This can be explained as in this region, k is almost constant since the DPSS curves are mainly “continuous” (see Appendix B). Hence, regardless of the error associated with E_t , the changes in k are minor. On the other hand, near the band edges, since the DPSS curves are “split” (see Appendix B), the error in the determined k value is relatively high. Extending the lower bound of the measurement temperature increases the range of E_t that at least one continuous DPSS curve is present, hence, decreasing the error in the extracted k near the band edges (see Appendix B). Generation of similar error maps can be helpful to better assess the validity of any extracted parameters from TIDLS measurements (considering the expected defect parameters, doping level, measurement temperature range, noise level, etc.). It should be noted that the error associated with temperature-dependent k is not considered in these simulations. However, this is a fundamental limit that also affects lifetime-based TIDLS measurements [6].

It seems that the different temperature ranges do not introduce a systematic error when extracting $[E_t, k]$ values in most areas, meaning that the Sun-V_{oc}(T)-based TIDLS method is not limited by the temperature range in the majority of the cases. The errors associated with the extracted E_t and k for both BO-related defect (white circle) and LID-related defect in Ga-doped cell (red circle) can be estimated from the above figures. It seems that only a very small difference in errors is present after changing the measurement temperature (below 0.02 eV for E_t and <4% for k).

Uncertainty in the measured temperature can also have an impact on the extracted parameters, as the calculated Δn is strongly correlated with the square of n_i [see Eq. (1)]. As n_i has a strong temperature dependency [27] a small error in the temperature measurement can lead to a significant error in n_i and thus, Δn . We, therefore, assessed the error in the temperature measurements by measuring the cell temperature with two thermocouples five times and determined a mean standard

deviation of only 0.6 °C and a maximum standard deviation of 1.5 °C (at 135 °C). Thus, it can be concluded that this effect does not impact the measurements in this study (see Appendix C).

A possible limitation of the proposed method is that the internal voltage and terminal voltage are not always similar [39] however, this effect is more dominant at higher light intensities (injections) while the change in the lifetime due to the bulk defects mainly happen in the low and medium injection ranges [8]. Another possible limitation of using the proposed method is shunted cells or high recombination at the metal and silicon interface [29,40,41]. However, the shunt resistance in modern industrial solar cells is often very high and the silicon-metal recombination is significantly reduced and predicted to be reduced even further with the implementation of passivating contacts like tunnel oxide passivated carrier-selective contacts (TOPCon) and heterojunction solar cells [42,43]. These improvements have made the use of Sun-V_{oc}(T) for defect analysis increasingly more possible.

4. Conclusions

In this study, a method based on Sun-V_{oc}(T) has been introduced to characterize defects within metalized cells. First, the method was validated by comparing the parameters of the BO-related defect extracted from a B-doped cell using the proposed method and from wafers using a conventional lifetime-based TIDLS method. The extracted parameters in the upper bandgap half ($E_t - E_i = 0.17 \pm 0.02$ eV and $k = 11.8 \pm 0.2$) were found to be similar to the parameters extracted from a wafer (the same E_t, k within 50%) and to the parameters reported in the literature (E_t within 14%, k within 25%). Then, the proposed method was utilized to extract the parameters of the defect causing LID in the Ga-doped cells. For the cells investigated in this study, the defect parameters were determined to be $E_t - E_i = -0.26 \pm 0.04$ eV and $k = 34 \pm 2$. Sensitivity analysis of the technique revealed that the limited temperature range of the system does not introduce a significant systematic error to the extracted parameters. Thus, it can be suggested that the uncertainty in the extracted parameters is mainly due to the factors which also affect lifetime-based TIDLS measurements.

This study clearly demonstrates the potential of Sun-V_{oc}(T)-based TIDLS measurement as a simple and accurate method for fast bulk defect characterization from metalized cells in production lines. Combining

this method with appropriate simulations of error maps further improves the assessment of the extracted parameters.

Declaration of competing interest

The authors declare that they have no known competing financial interests or personal relationships that could have appeared to influence the work reported in this paper.

Acknowledgment

This work was supported by the Australian Government through the Australian Renewable Energy Agency (ARENA) under grants 2017/RND001 and ARENA 1-A060. The views expressed herein are not necessarily the views of the Australian Government, and the Australian Government does not accept responsibility for any information or advice contained herein.

Appendix A. Supplementary data

Supplementary data to this article can be found online at <https://doi.org/10.1016/j.solmat.2021.111530>.

References

- [1] S. Rein, S. Glunz, Electronic properties of the metastable defect in boron-doped Czochralski silicon: unambiguous determination by advanced lifetime spectroscopy, *Appl. Phys. Lett.* 82 (2003) 1054–1056.
- [2] S. Diez, S. Rein, T. Roth, S. Glunz, Cobalt related defect levels in silicon analyzed by temperature-and injection-dependent lifetime spectroscopy, *J. Appl. Phys.* 101 (2007), 033710.
- [3] S. Bernardini, T.U. Nærland, A.L. Blum, G. Coletti, M.I. Bertoni, Unraveling bulk defects in high-quality c-Si material via TIDLS, *Prog. Photovoltaics Res. Appl.* 25 (2017) 209–217.
- [4] C. Vargas, Y. Zhu, G. Coletti, C. Chan, D. Payne, M. Jensen, Z. Hameiri, Recombination parameters of lifetime-limiting carrier-induced defects in multicrystalline silicon for solar cells, *Appl. Phys. Lett.* 110 (2017), 092106.
- [5] Y. Zhu, F. Rougier, N.E. Grant, J.A.T. De Guzman, J.D. Murphy, V.P. Markevich, G. Coletti, A.R. Peaker, Z. Hameiri, Electrical characterization of thermally activated defects in n-type Float-Zone silicon, *IEEE J. Photovol.* 11 (2020) 26–35.
- [6] S. Rein, Lifetime Spectroscopy: A Method of Defect Characterization in Silicon for Photovoltaic Applications, Springer Science & Business Media, 2006.
- [7] S. Rein, T. Rehrl, W. Warta, S. Glunz, Lifetime spectroscopy for defect characterization: systematic analysis of the possibilities and restrictions, *J. Appl. Phys.* 91 (2002) 2059–2070.
- [8] W. Shockley, W. Read Jr., Statistics of the recombinations of holes and electrons, *Phys. Rev.* 87 (1952) 835.
- [9] R.A. Sinton, A. Cuevas, M. Stuckings, Quasi-steady-state photoconductance, a new method for solar cell material and device characterization, in: 25th IEEE Photovoltaic Specialists Conference (PVSC), IEEE, 1996, pp. 457–460.
- [10] D.K. Schroder, Semiconductor Material and Device Characterization, John Wiley & Sons, 2015.
- [11] J. Giesecke, B. Michl, F. Schindler, M. Schubert, W. Warta, Minority carrier lifetime of silicon solar cells from quasi-steady-state photoluminescence, *Sol. Energy Mater. Sol. Cells* 95 (2011) 1979–1982.
- [12] R. Dumbrell, M.K. Juhl, T. Trupke, Z. Hameiri, Extracting metal contact recombination parameters from effective lifetime data, *IEEE J. Photovol.* 8 (2018) 1413–1420.
- [13] R.A. Sinton, A. Cuevas, A quasi-steady-state open-circuit voltage method for solar cell characterization, in: 16th European Photovoltaic Solar Energy Conference, EUPVSEC, 2000, p. 4.
- [14] D. Macdonald, A. Cuevas, Trapping of minority carriers in multicrystalline silicon, *Appl. Phys. Lett.* 74 (1999) 1710–1712.
- [15] P.J. Cousins, D.H. Neuhaus, J.E. Cotter, Experimental verification of the effect of depletion-region modulation on photoconductance lifetime measurements, *J. Appl. Phys.* 95 (2004) 1854–1858.
- [16] S.T. Sondergaard, J.O. Odden, R. Strandberg, Temperature dependent Suns-Voc of multicrystalline silicon solar cells from different ingot positions, in: 7th World Conference on Photovoltaic Energy Conversion (WCPEC), IEEE, 2018, pp. 2244–2247.
- [17] A.C. Killam, J.F. Karas, A. Augusto, S.G. Bowden, Monitoring of photovoltaic system performance using outdoor Suns-Voc, *Joule* 5 (2021) 210–227.
- [18] A.H.T. Le, R. Basnet, D. Yan, W. Chen, N. Nandakumar, S. Duttagupta, J.P. Seif, Z. Hameiri, Temperature-dependent performance of silicon solar cells with polysilicon passivating contacts, *Sol. Energy Mater. Sol. Cells* 225 (2021) 111020.
- [19] T. Niewelt, J. Schön, W. Warta, S.W. Glunz, M.C. Schubert, Degradation of crystalline silicon due to boron–oxygen defects, *IEEE J. Photovol.* 7 (2016) 383–398.
- [20] M. Fischer, M. Woodhouse, S. Herritsch, J. Trube, International Technology Roadmap for Photovoltaic (ITRPV), Technical Report, 2021.
- [21] S. Glunz, S. Rein, J. Knobloch, W. Wetting, T. Abe, Comparison of boron-and gallium-doped p-type Czochralski silicon for photovoltaic application, *Prog. Photovoltaics Res. Appl.* 7 (1999) 463–469.
- [22] N.E. Grant, J.R. Scowcroft, A.I. Pointon, M. Al-Amin, P.P. Altermatt, J.D. Murphy, Lifetime instabilities in gallium doped monocrystalline PERC silicon solar cells, *Sol. Energy Mater. Sol. Cells* 206 (2020) 110299.
- [23] N.E. Grant, P.P. Altermatt, T. Niewelt, R. Post, W. Kwapił, M.C. Schubert, J. D. Murphy, Gallium-doped silicon for high-efficiency commercial passivated emitter and rear solar cells, *Solar RRL* 5 (2021) 2000754.
- [24] Z. Hameiri, N. Borjevic, L. Mai, N. Nandakumar, K. Kim, S. Winderbaum, Low-absorbing and thermally stable industrial silicon nitride films with very low surface recombination, *IEEE J. Photovol.* 7 (2017) 996–1003.
- [25] Y. Zhu, Z. Hameiri, Review of injection dependent charge carrier lifetime spectroscopy, *Progress in Energy* 3 (2021), 012001.
- [26] R.A. Sinton, A. Cuevas, Contactless determination of current-voltage characteristics and minority-carrier lifetimes in semiconductors from quasi-steady-state photoconductance data, *Appl. Phys. Lett.* 69 (1996) 2510–2512.
- [27] R. Couderc, M. Amara, M. Lemiti, Reassessment of the intrinsic carrier density temperature dependence in crystalline silicon, *J. Appl. Phys.* 115 (2014), 093705.
- [28] A. Cuevas, The effect of emitter recombination on the effective lifetime of silicon wafers, *Sol. Energy Mater. Sol. Cells* 57 (1999) 277–290.
- [29] J. Müller, K. Bothe, S. Gatz, H. Plagwitz, G. Schubert, R. Brendel, Contact formation and recombination at screen-printed local aluminum-alloyed silicon solar cell base contacts, *IEEE Trans. Electron. Dev.* 58 (2011) 3239–3245.
- [30] Y. Tomizawa, Y. Ikeda, H. Itoh, T. Shiro, J. Löffler, P. Manshanden, I. Romijn, Analysis of contact recombination at rear local back surface field via boron laser doping and screen-printed aluminum metallization on p-type PERC solar cells, *Energy Procedia* 124 (2017) 384–391.
- [31] N. Nampalli, H. Li, M. Kim, B. Stefani, S. Wenham, B. Hallam, M. Abbott, Multiple pathways for permanent deactivation of boron–oxygen defects in p-type silicon, *Sol. Energy Mater. Sol. Cells* 173 (2017) 12–17.
- [32] J. Schmidt, A. Cuevas, Electronic properties of light-induced recombination centers in boron-doped Czochralski silicon, *J. Appl. Phys.* 86 (1999) 3175–3180.
- [33] S. Boughaba, D. Mathiot, Deep level transient spectroscopy characterization of tungsten-related deep levels in silicon, *J. Appl. Phys.* 69 (1991) 278–283.
- [34] B. Paudyal, K. McIntosh, D. Macdonald, Temperature dependent carrier lifetime studies on Ti-doped multicrystalline silicon, *J. Appl. Phys.* 105 (2009) 124510.
- [35] J. Schmidt, B. Lim, D. Walter, K. Bothe, S. Gatz, T. Dullweber, P.P. Altermatt, Impurity-related limitations of next-generation industrial silicon solar cells, in: 38th IEEE Photovoltaic Specialists Conference, PVSC, 2012.
- [36] K. Graff, Metal Impurities in Silicon-Device Fabrication, Springer Science & Business Media, 2013.
- [37] D. Lin, Z. Hu, L. Song, D. Yang, X. Yu, Investigation on the light and elevated temperature induced degradation of gallium-doped Cz-Si, *Sol. Energy* 225 (2021) 407–411.
- [38] Y. Buratti, Q.T. Le Gia, J. Dick, Y. Zhu, Z. Hameiri, Extracting bulk defect parameters in silicon wafers using machine learning models, *npj Computational Materials* 6 (2020) 1–8.
- [39] R. Dumbrell, M.K. Juhl, T. Trupke, Z. Hameiri, Comparison of terminal and implied open-circuit voltage measurements, *IEEE J. Photovol.* 7 (2017) 1376–1383.
- [40] M.A. Green, Solar cell minority carrier lifetime using open-circuit voltage decay, *Sol. Cell.* 11 (1984) 147–161.
- [41] F.W. Chen, J.E. Cotter, M.D. Abbott, T.-T.A. Li, K.C. Fisher, The influence of parasitic effects on injection-level-dependent lifetime data, *IEEE Trans. Electron. Dev.* 54 (2007) 2960–2968.
- [42] S. De Wolf, A. Descoeuadres, Z.C. Holman, C. Ballif, High-efficiency silicon heterojunction solar cells: a review, *green* 2 (2012) 7–24.
- [43] F. Feldmann, M. Bivour, C. Reichel, M. Hermle, S.W. Glunz, Passivated rear contacts for high-efficiency n-type si solar cells providing high interface passivation quality and excellent transport characteristics, *Sol. Energy Mater. Sol. Cells* 120 (2014) 270–274.